

Supplement of

Shipborne measurements of ClNO₂ in the Mediterranean Sea and around the Arabian Peninsula during summer

Philipp G. Eger et al.

5 *Correspondence to:* John N. Crowley (john.crowley@mpic.de)

Corrections to the aerosol particle surface area concentration

To derive the ambient PM_1 particle surface area concentration A from the measured dry particle surface area concentration (AMS) we applied a hygroscopic growth factor based on ambient RH and PM_1 aerosol composition. From the AMS measurements we derived the molar ratio of sulphate to ammonium of ≈ 2.2 (see Fig. S1), which is close to the ratio of ≈ 2 for completely neutralised ammonium-sulphate aerosol, indicating its dominance in the fine mode during AQABA. For most of the campaign $(NH_4^+)_2(SO_4^{2-})$ contributed 80-100 % to the total inorganic PM_1 aerosol mass (see Fig. S2) while nitrate and chloride were less abundant. A relative humidity-dependent growth factor G_{amsu} for the particle diameter was calculated using the parameterisation (Eq. S1) of Lewis (2008) for pure ammonium-sulphate drops with $a = 0.78$ and $b = 1.90$.

$$10 \quad G_{amsu}(RH) = a \left(b + \frac{1}{1-RH} \right)^{1/3} \quad (S1)$$

The growth factor was calculated considering the RH of the sample air after passing the aerosol dryer (see Sect. 2.5 in the manuscript) which was usually in the range 40 ± 10 %. To account for the organic mass fraction we calculated the volume fraction v_{org} of organics using a typical density of 1400 kg/m^3 for oxidised organics in aged atmospheric aerosol (Gysel et al., 2007) and the volume fraction v_{amsu} of $(NH_4^+)_2(SO_4^{2-})$, assuming that all NH_4^+ and SO_4^{2-} measured originated from ammonium-sulphate. In the next step we derived a combined growth factor by applying a mixing rule (Eq. S2) where the water activity a_w was approximated by the relative humidity (Gysel et al., 2007):

$$15 \quad G_{mixed} \approx \left(\sum_i v_i G_i^3 \right)^{1/3} \quad (S2)$$

20 For the organic fraction a growth factor of $G_{org} = 1.20 \pm 0.10$ at $a_w = 0.9$ and a ratio of $\frac{G_{org}}{G_{amsu}} \approx \frac{1.20}{1.80}$ was reported by Gysel et al. (2007). Assuming a similar RH -dependence for G_{org} than for G_{amsu} results in Eq. S3 which can be inserted into Eq. S2 along with Eq. S1.

$$G_{org} \approx 1 + \frac{1}{4}(G_{amsu} - 1) \quad (S3)$$

25 The resulting surface area growth factor $G_A = (G_{mixed})^2$ as a function of RH is shown in Fig. S3. The particle surface area concentration (PM_1) reported in Table 1 of the manuscript already includes this correction. The distribution of surface area growth factors for the whole AQABA campaign is shown in Fig. S4 and has a campaign average of 1.32 ± 0.24 .

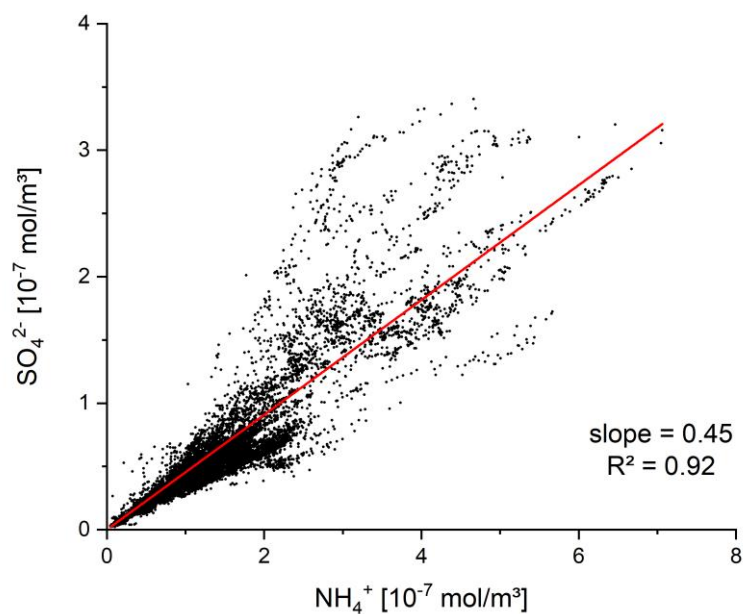


Figure S1: Correlation between PM₁ (AMS) ammonium and sulphate (in mol m⁻³).

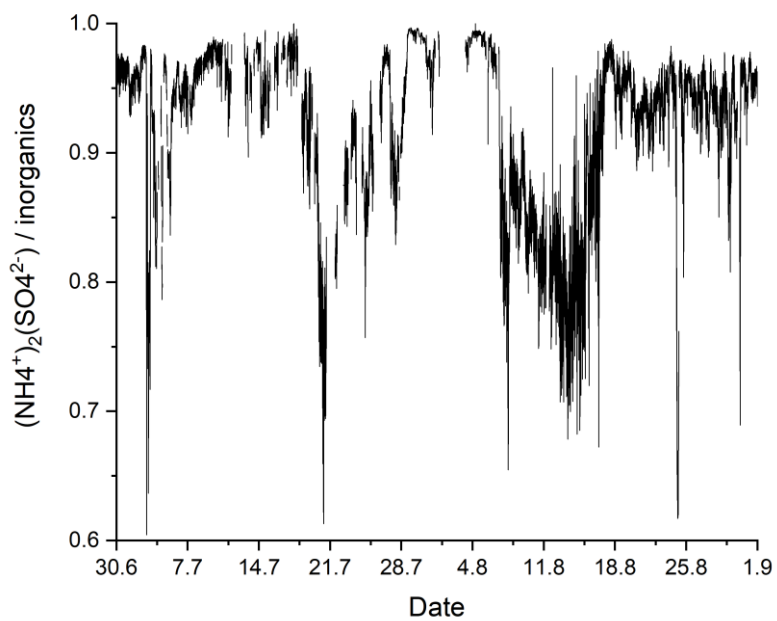


Figure S2: Contribution of ammonium-sulphate to the total non-refractory inorganic PM₁ aerosol mass.

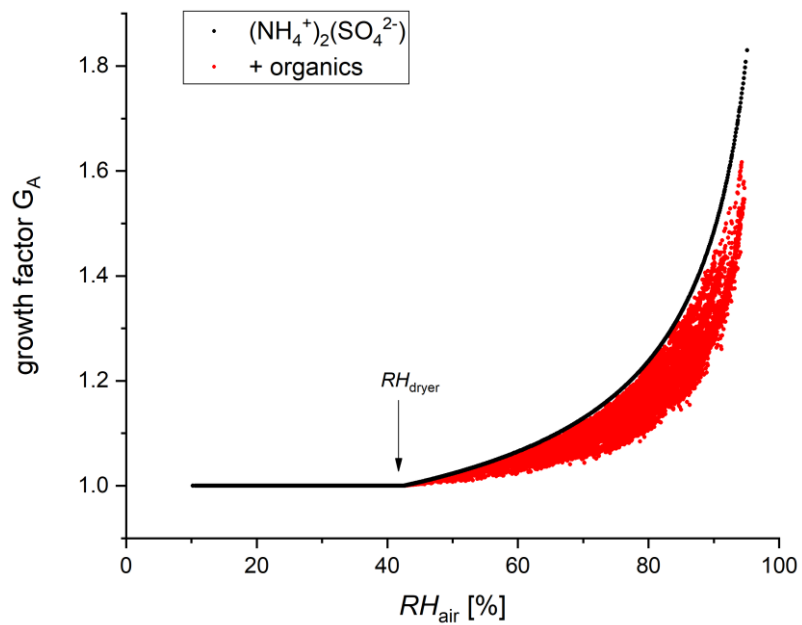


Figure S3: Surface growth factors for pure ammonium-sulphate (black) and for a mixture with organics (red).

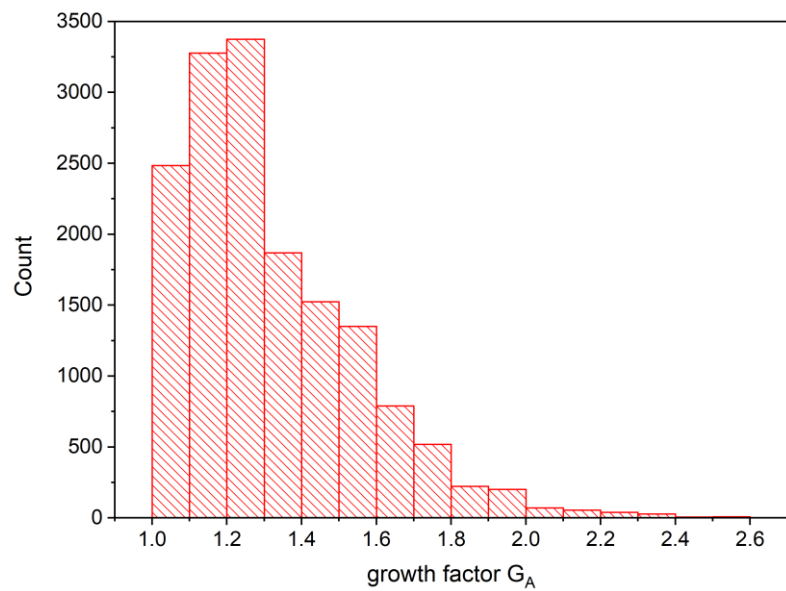


Figure S4: Distribution of calculated surface area growth factors G_A for the whole AQABA campaign.

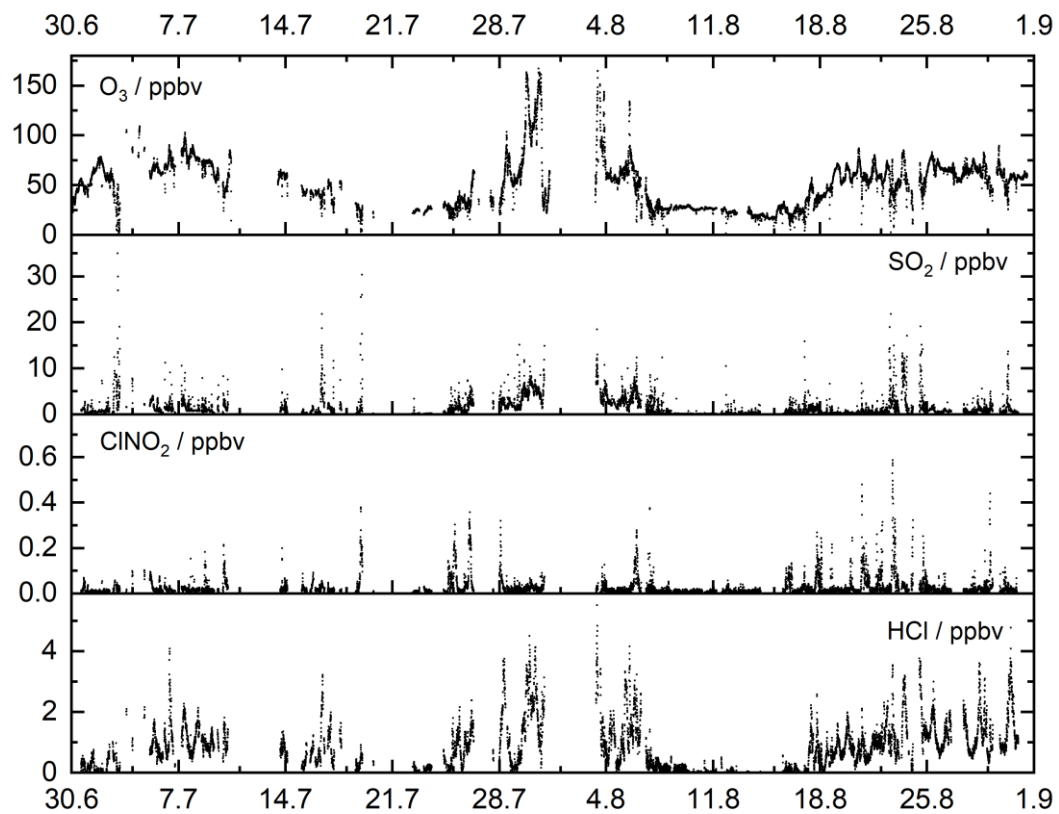
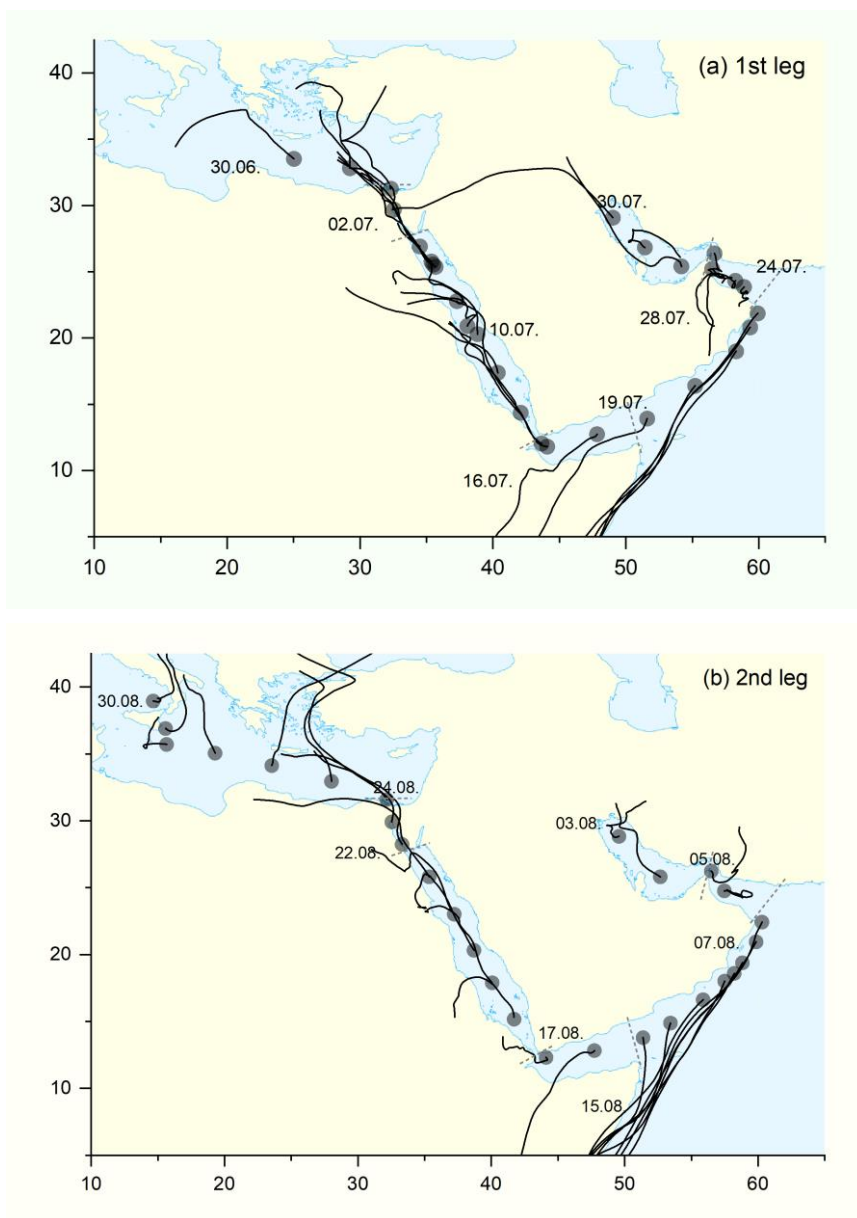


Figure S5: Time series of O_3 , SO_2 , $ClNO_2$ and HCl mixing ratios during the AQABA campaign.



5 **Figure S6:** 48-h back-trajectories calculated with HYSPLIT (at 100 m above sea-level) representative for the corresponding nights.

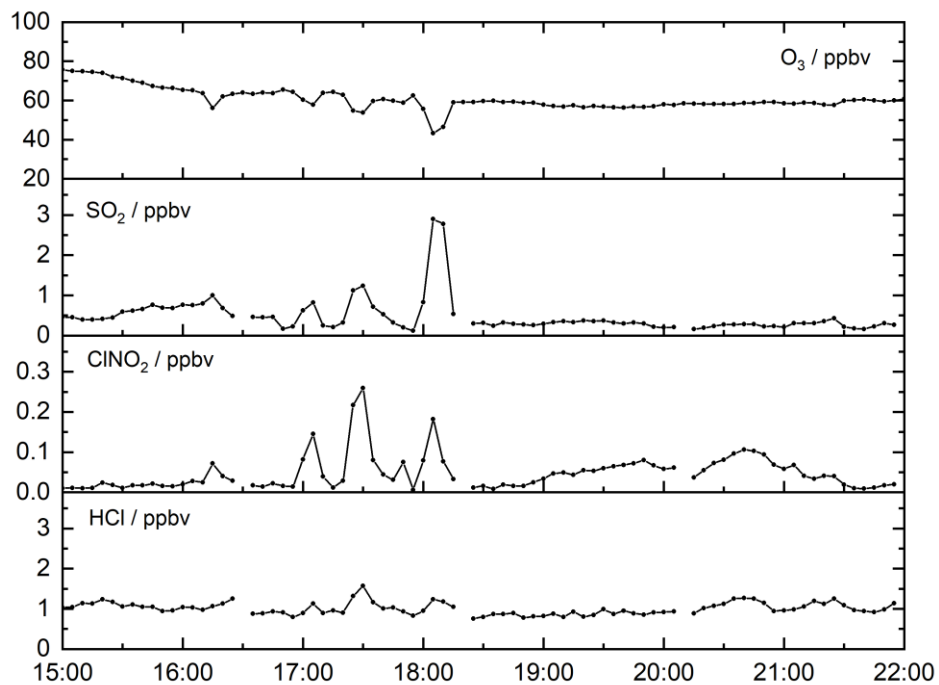


Figure S7: Observation of ClNO₂ in distinct ship plumes between 16:30 and 18:30 UTC (indicated by increased SO₂ mixing ratios and O₃ titration due to NO) on the 21st of August in the Red Sea.

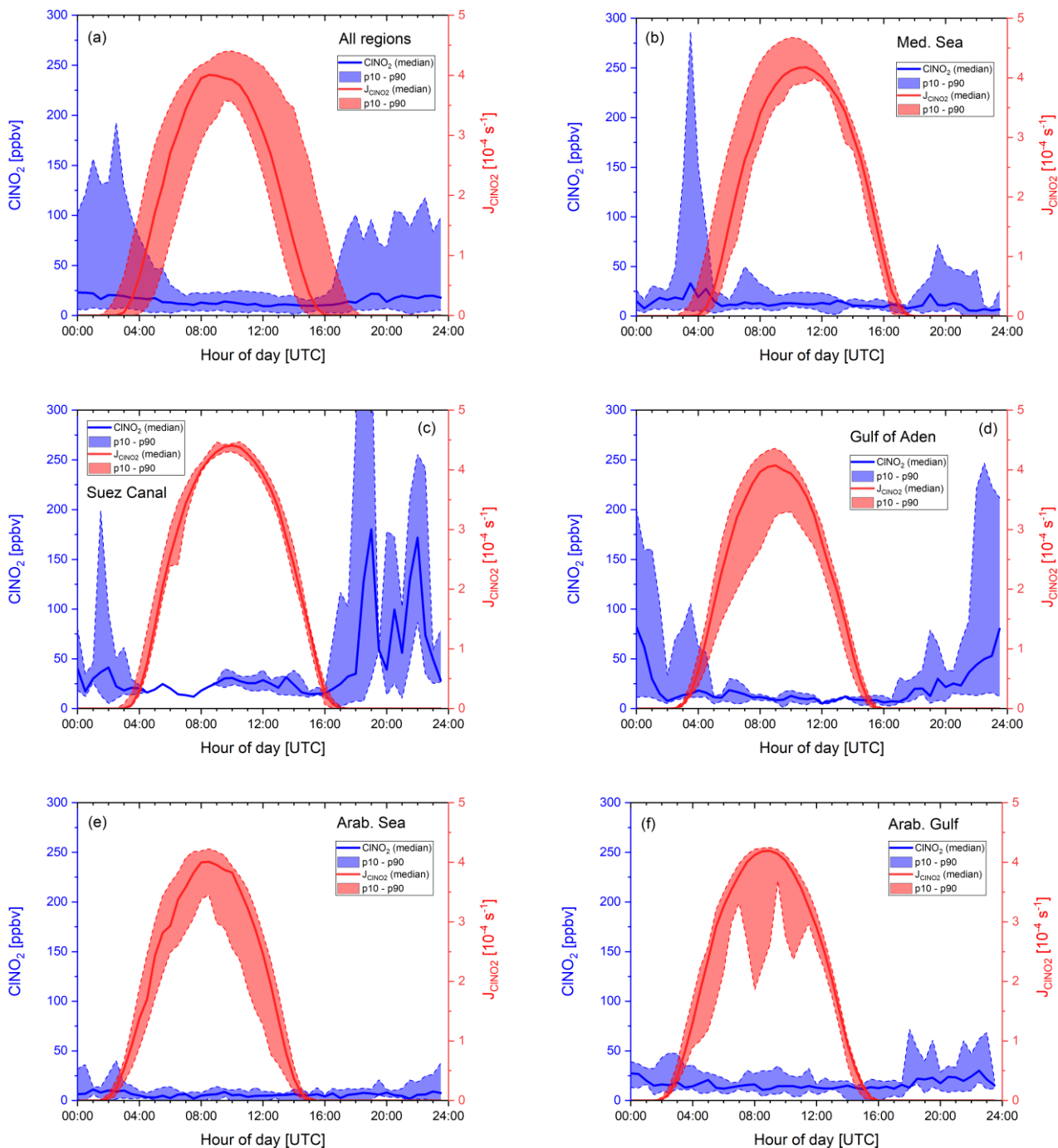


Figure S8: Diurnal profiles of ClNO_2 for (a) all regions combined, (b) the Mediterranean Sea, (c) the Suez Canal and Gulf of Suez, (d) the Gulf of Aden, (e) the Arabian Sea, and (f) the Arabian Gulf. p10 and p90 correspond to the 10th and 90th percentiles.

Additional details to the derivation of the ClNO₂ production efficiency ϵ

To investigate the uncertainty related to assumptions made in the calculation of ϵ , we define five different methods A-E and compare them to each other by applying them to the whole AQABA dataset (Fig. S9).

Method A: The starting point t_0 for NO₃ formation is set to sunset minus 40 ± 10 min as described in the manuscript but all data points before sunset were excluded from the analysis due to a large uncertainty in reaction time. This way 4175 values of ϵ were obtained throughout the campaign. In *Method A*, we inherently assume that the air mass we probe has not been influenced by fresh NO emissions since the beginning of the night. A fresh NO emission would mean that the air mass at the beginning of the night would have contained less NO₂ than calculated in Eq. 3 resulting in an overestimation of the integrated NO₃ production and thus values of ϵ calculated by *Method A* represent a lower limit.

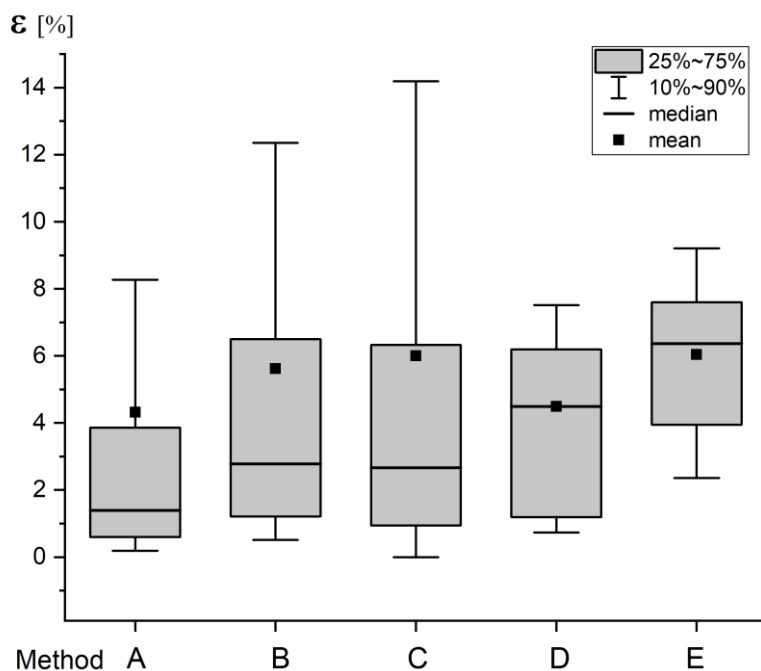
Method B: To account for fresh emissions of NO (e.g. by passing ships), the reaction time t' was calculated from Eq. 5 where s represents the number of NO₂ molecules required to make NO_y and is 1 when NO₃ reacts directly with VOCs and 2 when NO₃ reacts with NO₂ to form N₂O₅, which subsequently hydrolyses to HNO₃. As discussed later, the direct NO₃ losses are dominant throughout the campaign compared to the heterogeneous N₂O₅ production, so to a good approximation, $s = 1$. As discussed by McDuffie et al. (2018) inherent to the use of this expression is the assumption that NO_y is conserved during the night; any losses of NO_y (e.g. via deposition of HNO₃) leading to an underestimation of the true reaction time. Whenever t' is shorter than the time elapsed since sunset (see *Method A*), t' is used to integrate the NO₃ production term. As the calculated, night-time air mass age depends on the ratio between [NO₂] and [NO_y], the calculation breaks down whenever a fresh NO emission (e.g. from a nearby ship) is injected into an air-mass and unreacted NO is still present. In this case the NO₂ to NO_y ratio would be decreased and the age of the air-mass overestimated. To avoid this, we only use data where NO is below the detection limit, resulting in a total number of $N_B = 2987$ data points.

Method C: Here we only consider data points where the calculated age of the air mass (as derived in *Method B*) is equal to or exceeds the time elapsed since sunset as derived in *Method A*. These air masses are unlikely to have been impacted by recent emission. As loss of NO₂ by deposition will result in an air mass age that is shorter than the true one, we relax the criterion for equality of reaction times by also including calculated air mass ages that are up to 25 % shorter (i.e. $t' \geq 0.75 (t - t_0)$). The resulting dataset is reduced to $N_C = 1742$ data points. All values of ϵ discussed in the manuscript were derived using method C.

Method D: ClNO₂ mixing ratios close to the limit of detection (LOD) result in a higher uncertainty and variability in ϵ , especially when the NO₃ production term is also small. In *Method D*, we use only data in which the ClNO₂ mixing ratio is at least 25 pptv, which represents the LOD + the median, daytime HCl-interference (Sect. 3.1). This drastically reduces the size of the dataset to $N_D = 280$ data points.

Method E: In method E, we examine the efficiency of ClNO_2 formation only during a few nights when its mixing ratio exceeded 100 pptv. The intention here is not to derive e.g. a regional mean value, but to indicate that even when biasing the dataset to apparently efficient ClNO_2 generation, ϵ remains low. In Method E, only 50 data points remain (1.2% of the dataset analysed in *Method A*).

- 5 We summarise values of ϵ as median and mean values for the entire campaign in Fig. S9, segregated into the five different methods used to select data and derive the reaction time. As described earlier, *Method A* can be understood as a lower limit for ϵ providing a median efficiency of only 1.4 % with a range from 0–8 % (10th and 90th percentiles) and a large difference between mean and median values. More reliable median values of $\epsilon = 2.8 \%$ and 2.7% are provided by *Methods B and C*. *Method D*, results in identical median and mean values of $\epsilon = 4.5 \%$, although a bias towards higher values is difficult to rule out as low ClNO_2 mixing ratios were excluded. For *Method E*, where we only consider data with $\text{ClNO}_2 > 100$ pptv, we derive a larger median value of $\epsilon = 6.4 \%$. If we consider only the individual maxima in the ClNO_2 mixing ratio (above 100 pptv) on any particular night, we derive 17 values of ϵ that vary between 1.1 and 11.2 % which are listed in Table S1.
- 10 In our manuscript (Fig. 5 and 6) we exclusively report values of ϵ derived by method C. In comparison to Fig. 6 in the manuscript, Figure S10 illustrates how the box-plots for the seven regions would be altered when applying method D instead of method C. The variability is generally decreased and median values are shifted towards higher values, but the general picture and conclusions are not changed.
- 15



20 **Figure S9:** Box plot of ϵ derived by the different methods A–E for the whole AQABA campaign. The whiskers represent the 10th and 90th percentiles.

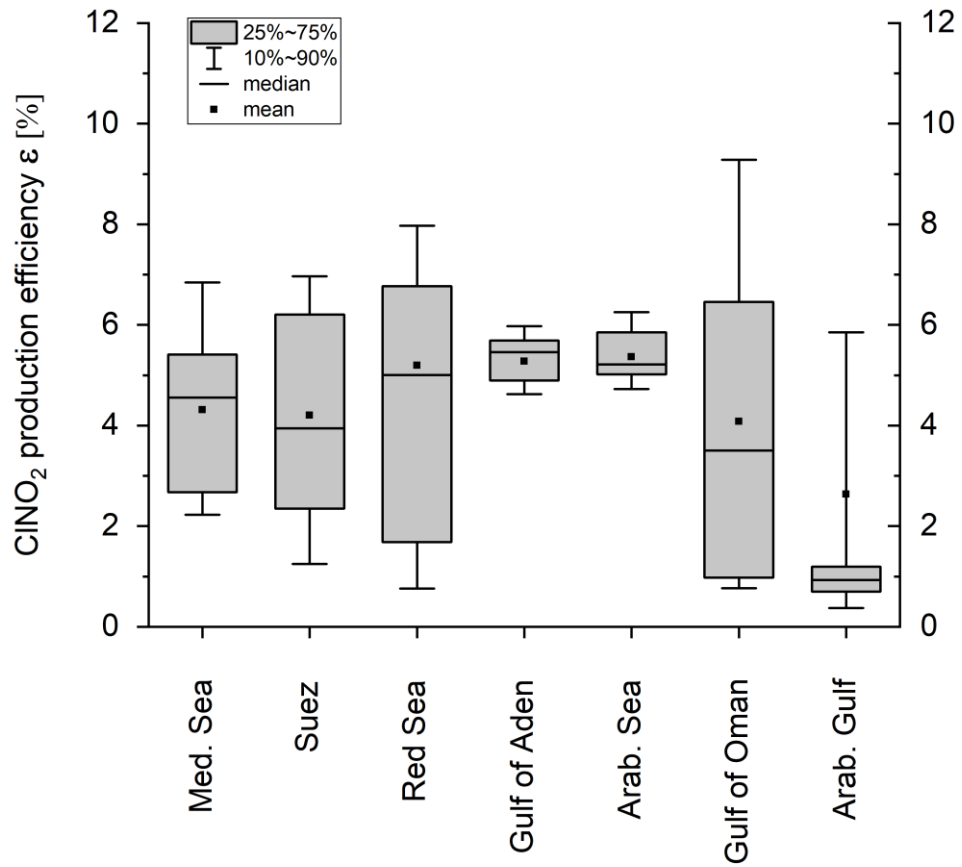


Figure S10: Median values of ϵ (CINO₂ production efficiency) for each region, calculated from individual night-time values (between 10 and 104 per region) based on Eq. 4 in the manuscript but using method D instead of method C.

5

10

Table S1: Observed ClNO₂ plumes ¹ (typical duration of one to several hours) with mixing ratios above 100 pptv.

Date, time / UTC	Region	t / h	t' / h	ClNO ₂ / pptv	N ₂ O ₅ / pptv	NO _{3, int} / ppbv	ϵ / %	O ₃ / ppbv	SO ₂ / ppbv	HCl / ppbv	NO ₂ / ppbv
08.07. 17:50	Red Sea	1.8	1.5	128	-	3.17	4.0	61.5	3.0	1.1	6.9
24.07. 16:05	Oman	1.8	2.3	143	-	1.28	1.1	25.7	1.1	0.3	7.0
03.08. 18:00	Arab. Gulf	2.9	2.6	115	53	9.65	1.2	78.8	3.0	1.8	6.7
06.08. 18:45	Oman	4.3	3.9	173	-	1.55	1.1	28.1	1.4	0.7	2.9
06.08. 20:35	Oman	6.1	6.9	159	-	2.86	5.6	20.0	4.0	0.6	5.2
17.08. 18:00	Red Sea	3.0	4.5	120	9	1.54	7.8	34.4	1.6	0.7	3.2
17.08. 19:25	Red Sea	4.4	3.6	212	14	3.03	7.0	34.7	2.1	1.8	3.9
17.08. 20:05	Red Sea	5.1	4.7	168	8	2.03	8.3	32.0	1.3	1.5	2.4
18.08. 17:00	Red Sea	1.8	1.5	106	23	1.49	7.1	42.9	0.9	0.6	4.6
20.08. 16:45	Red Sea	1.3	1.0	144	59	1.90	7.6	58.7	0.7	1.0	5.8
21.08. 17:05	Red Sea	1.5	1.4	145	53	2.13	6.8	57.9	0.8	1.1	5.9
21.08. 17:30	Red Sea	1.9	2.5	259	87	3.14	8.2	53.8	1.2	1.6	7.1
21.08. 23:40	Red Sea	8.1	8.5	103	27	9.78	1.1	58.0	0.7	1.1	2.3
22.08. 16:50	Suez	1.0	1.3	123	118	1.96	6.3	45.7	2.5	1.2	11.4
22.08. 18:20	Suez	2.5	2.1	586	355	7.09	8.3	56.4	4.6	3.5	11.3
22.08. 21:40	Suez	5.8	4.6	308	52	8.77	3.5	39.4	1.2	1.2	7.6
22.08. 22:30	Suez	6.7	6.1	222	47	9.45	2.3	43.0	1.0	1.1	5.9

¹ Regions: Red Sea, Gulf of Oman (Oman), Arabian Gulf (Arab. Gulf) and Suez Canal / Gulf of Suez (Suez). t denotes the time since sunset; t' corresponds to the air mass age calculated from Eq. 5 in the manuscript NO_{3, int} is the total amount of NO₃ produced over the course of the night and ϵ is the ClNO₂ production efficiency (Eq. 4 in manuscript).

References

- 5 Gysel, M., Crosier, J., Topping, D., Whitehead, J., Bower, K., Cubison, M., Williams, P., Flynn, M., McFiggans, G., and
Coe, H.: Closure study between chemical composition and hygroscopic growth of aerosol particles during TORCH2, *Atmos.*
Chem. Phys., 7, 6131-6144, 2007.
- 10 Lewis, E. R.: An examination of Köhler theory resulting in an accurate expression for the equilibrium radius ratio of a
hygroscopic aerosol particle valid up to and including relative humidity 100%, *Journal of Geophysical Research:*
Atmospheres, 113, 2008.
- 15 McDuffie, E. E., Fibiger, D. L., Dubé, W. P., Lopez-Hilfiker, F., Lee, B. H., Thornton, J. A., Shah, V., Jaeglé, L., Guo, H.,
and Weber, R. J.: Heterogeneous N_2O_5 uptake during winter: Aircraft measurements during the 2015 WINTER campaign
and critical evaluation of current parameterizations, *Journal of Geophysical Research: Atmospheres*, 123, 4345-4372, 2018.